Published in final edited form as:
Adv Mater. 2008 May 5; 20(9): 1630–1635. doi:10.1002/adma.200800004.

Magnetic Iron Oxide Nanoworms for Tumor Targeting and Imaging**

Ji-Ho Park,
Materials Science and Engineering Program, Department of Chemistry and Biochemistry, University of California, San Diego, 9500 Gilman, La Jolla, CA 92093 (USA)

Geoffrey von Maltzahn,
Harvard–MIT Division of Health Sciences and Technology, Massachusetts Institute of Technology, 77 Massachusetts Avenue, Cambridge, MA 02139 (USA)

Lianglin Zhang,
Burnham Institute for Medical Research at UCSB, University of California, Santa Barbara, 1105 Life Sciences Technology Bldg., Santa Barbara, CA 93106 (USA)

Michael P. Schwartz,
Materials Science and Engineering Program, Department of Chemistry and Biochemistry, University of California, San Diego, 9500 Gilman, La Jolla, CA 92093 (USA)

Erkki Ruoslahti,
Burnham Institute for Medical Research at UCSB, University of California, Santa Barbara, 1105 Life Sciences Technology Bldg., Santa Barbara, CA 93106 (USA)

Sangeeta N. Bhatia, and
Harvard–MIT Division of Health Sciences and Technology, Massachusetts Institute of Technology, 77 Massachusetts Avenue, Cambridge, MA 02139 (USA)

Michael J. Sailor*
Materials Science and Engineering Program, Department of Chemistry and Biochemistry, University of California, San Diego, 9500 Gilman, La Jolla, CA 92093 (USA)

The application of nanotechnology to medicine is providing new approaches for the diagnosis and treatment of diseases.[1–14] Ultrasensitive imaging for early detection of cancers and efficient delivery of therapeutics to malignant tumors are two primary goals in cancer bionanotechnology; however, the development of nontoxic, functional nanoparticles that can successfully home to tumors presents some significant challenges. Dextran-coated magnetic iron oxide (IO) nanoparticles are of particular interest because they show relatively low toxicity and long circulation, and dramatically enhance hydrogen T_2 relaxation in magnetic resonance imaging (MRI).[5,11,15–20] The clinical power of these materials may be amplified by improving MRI relaxivity, blood circulation times, and the homing of such nanoparticles to tumors. Efforts to increase MRI sensitivity have focused on development of new magnetic core materials,[6,12] or on improvements in nanoparticle size[21] or

**This project has been funded in part with Federal funds from the National Cancer Institute of the National Institutes of Health (Contract No. N01-C0-37117 and R01CA124427-01). M.J.S., E.R., and S.N.B. are members of the Moores UCSD Cancer Center and the UCSD NanoTUMOR Center under which this research was conducted and partially supported by NIH Grant U54 CA 119335. J.P. thanks the Korea Science and Engineering Foundation (KOSEF) for a Graduate Study Abroad Scholarship. The authors thank Todd Sponholtz and Dr. Ralph Weissleder for use of the NIR fluorescence-imaging system, and Dr. Edward Monosov for assistance with TEM analysis.

*msailor@ucsd.edu.

clustering.[7,22] However, most efforts to improve the morphological characteristics of these nanoparticles have resulted in materials with relatively short circulation half-lives owing to incomplete additional hydrophilic coatings.[6,12,21]

An emerging theme in nanoparticle research is to control biological behavior and/or electromagnetic properties by controlling shape. The manipulation of electrical, magnetic, and optical properties by controlling the shape of nanomaterials has been demonstrated in many areas.[23–25] There are, however, limited studies that point to a shape dependence of the in vitro or in vivo behavior of nanomaterials.[14,26–28] One of the most important pathways for clearance of nanoparticles in vivo is the mononuclear phagocytic system (MPS). At the micrometer scale, particle shape is known to play a dominant role in particle uptake by phagocytes.[26] Some types of elongated nanoparticles have been shown to exhibit low MPS uptake and, as a result, prolonged blood half-life relative to spherical shapes.[13,14,29] For example, spherical micelles are taken up by phagocytes more readily than micelles that have been extended into filaments by shear flow.[14] Conversely, for targeted materials, elongation enhances the surface-to-volume ratio, allowing polyvalent binding to amplify particle affinity for cell surface receptors.[13,30]

In this work, we hypothesized that a nanostructure with an elongated assembly of IO cores (referred to here as nanoworms, NWs) would improve the ability of the nanoparticles to circulate, target, and image tumors. The synthetic strategy is inspired by the previous observation that magnetic nanoparticles can become aligned along strands of high-molecular-weight dextran.[31] We find that the geometry of the nanoparticles (elongated versus spherical) influences their efficacy both in vitro and in vivo by enhancing their magnetic relaxivity in MRI, increasing their ability to attach to tumor cells in vitro owing to enhanced multivalent interactions between peptide-modified NW and cell receptors, and amplifying their passive accumulation in vivo over spherical nanoparticle controls.

The NW synthesis is similar to the typical preparation of magnetic IO nanospheres (NSs), involving the reaction of Fe(II) and Fe(III) salts in the presence of dextran.[32] In order to prepare the wormlike morphology, the concentrations of iron salts are higher and the molecular weight of dextran is larger (20 kDa). The nanostructure appears in the transmission electron microscopy (TEM) image (Fig. 1a) as a string of IO cores (ca. 5 nm diameter) with an overall length on the order of 50 nm. The mean hydrodynamic size, measured by dynamic light scattering (DLS) is 65nm (Table 1). It is not clear from the data if the IO cores are in contact with each other or merely in close proximity. When higher-molecular-mass dextran (40 kDa) is used, highly branched IO cores, with a larger size (~100 nm) and a broader size distribution (Supporting Information Fig. 1) are obtained.

To provide comparison, nanospheres were synthesized using a published procedure.[32] They exhibited physical sizes and shapes, magnetic responses, and biological properties similar to what has been previously reported (Fig. 1,Table 1, and Supporting Information Fig. 2a).[15–18,32] NWs are characterized as elongated, dextrancoated particles composed of a linear aggregate of 5–10 IO cores (50–80 nm) while NSs are spherical, dextran-coated particles containing 1–2 IO cores (25–35 nm). NWs display a slightly larger saturation magnetization value (74.2 emu g_{Fe}^{-1} versus 61.5 emu g_{Fe}^{-1} Fe and 53.5 emu g_{Fe}^{-1}) and higher MR contrast (R_2 = 116 $mMFe^{-1}$ S^{-1} versus R_2 = 70 $mMFe^{-1}$ S^{-1} and R_2 =95 $mMFe^{-1}$ S^{-1}) than NSs and the commercially available Feridex (Fig. 1b–d). The elongated structure of the NWs apparently enhances the orientation of the magnetic moments of the individual nanoparticle constituents, increasing the net magnetization.[33,34] The increased MR contrast observed for NWs is thought to be due to enhanced spin–spin relaxation of water molecules caused by the slightly larger magnetization value[12,21] and the 1D assembly.[22,35]

The efficiency of peptide-targeted cellular internalization of NW relative to NS was tested on MDA-MB-435 tumor cells in vitro. Conceptually, the elongated shape of the NWs is expected to provide a larger number of interactions between the targeting ligands and their cell-surface receptors compared with spherical nanoparticles (Fig. 2a). For this study, the internalizing peptide, F3, was used as the targeting species. F3 selectively targets cell-surface nucleolin in tumor cells and tumor endothelial cells, and is known to have cell-penetrating properties.[36–38] The number of peptides coupled to the particles was controlled by varying the extent of amination of the dextran coating (Table 1). Superconducting quantum interference device (SQUID) and fluorescence data indicate that internalization of F3-conjugated NWs (NW-F) is enhanced relative to F3-conjugated NS (NS-F) on a per-iron basis (Fig. 2b and Supporting Information Fig. 3a and b). For either NWs or NSs, the degree of internalization increases with the number of F3 peptides attached and incubation time, and dextran-coated NWs or NSs that do not contain targeting peptides display no evidence of internalization. Incorporation of a poly(ethylene glycol) (PEG) linker between the F3 targeting peptide and the NW reduces cellular uptake ofNW (Fig. 2b). In a competition study, equal amounts (iron basis) of NW-175-F and NS-30-F were co-incubated, and NWs were found to inhibit cellular uptake of NSs (Supporting Information Fig. 3c). NWs recovered 24 h after internalization in cells retained their original shape (Supporting Information Fig. 3d).

Circulation in the blood stream for a long period of time is a key requirement for in vivo target-specific reporting and drug delivery with nanomaterials.[20,39] We tested the blood circulation times of unmodified NWs and NSs with an injection dose of 3mg Fe kg^{-1} body mass in mice. Both exhibited similar long circulation times (blood half-lives: 15–18 h) with a first-order elimination rate (Fig. 3a and Table 1).[17] NWs extracted from the bloodstream after 24 h retained their original shape (Supporting Information Fig. 4) and they showed a slight increase in hydrodynamic size (from ca. 65 to ca. 80 nm by DLS), attributed to protein binding during circulation.

The biodistribution of NWs in the mouse 24 h post injection is similar to that reported previously for NSs.[17] These particles both display a tendency to undergo MPS clearance in the liver, spleen, and lymph nodes (Fig. 3b). However, there are some differences in the biodistribution of NWs relative to NSs. The fraction of injected particles in the kidney is lower relative to the liver for NWs compared with NSs, whereas the spleen:liver particle concentration ratio is higher for NW.

In circulation nanoparticles tend to passively accumulate in tumors, since tumor vessels are generally found to be more permeable than the vessels of healthy tissues.[2] Passive tumor uptake of NWs in mouse xenograft MDA-MB-435 tumors was greater than NS (Fig. 3c). Interestingly, NWs remain in the tumor 48 h after injection, whereas NS are almost completely eliminated within this time period. The clearance behavior of NS is similar to that observed with RGD-conjugated quantum dots, which are of a comparable size.[9] The data indicate that once NW extravasate into tumor tissue from the blood vessels, they become physically trapped and do not readily re-enter the blood stream. Thus more effective diagnostic imaging or drug delivery may be possible with NW than with NS.

High-aspect-ratio nanomaterials such as carbon nanotubes and worm micelles have been found to circulate long enough to enable homing to biological targets despite their micrometer-sized length.[13,14,29] In addition, pseudo-1D assemblies of nanocrystals can display desirable optical or magnetic properties not found in the isodimensional materials.[40] The linear aggregation of IO cores increases MRI sensitivity as shown in this study, suggesting that NWs may offer an improved ability to image very small or poorly vascularized tumors.

The mechanism by which iron cores become linearly aggregated during synthesis requires further study, although the key factor seems to the molecular mass of the dextran polymer. Several methods to construct 1D assemblies of nanocrystals have been reported in recent years, for example involving the use of molecular coatings or biotemplates.[40–42] These approaches provide a means to control the chain-like nanostructures more precisely, although in vivo properties of such materials have not yet been characterized.

There have been many studies comparing the targeting ability of multivalent with monovalent ligands on nanomaterials.[30,43,44] Here we have investigated the effect of nanoparticle morphology on intracellular delivery while attempting to maintain comparable surface chemical characteristics. For a constant ratio of attached targeting peptides per iron atom, NWs display a greater ability to be taken up by cultured tumor cells than NSs. The data suggest that the enhanced polyvalency of NWs versus NSs allows particles to bind to tumor cells with a higher avidity. No significant uptake is observed if the NWs or NSs contain no targeting peptides.

When shape and surface charge are held constant, the blood circulation time of nanoparticles is generally observed to decrease with increasing size.[39] However, nanomaterials that are elongated along one dimension seem to be better able to evade the organism's natural elimination processes.[13,14,29] This study clearly demonstrates that nanoparticle size can be increased along one dimension without sacrificing circulation time. The geometric alignment of cores within NW provides two key advantages over spherical counterparts: the elongated shape, with its larger surface area, presents multiple targeting ligands that can cooperatively interact with cell surfaces and linearly aggregated IO cores generate improved T_2 relaxivity for MR imaging. In addition, the nanomaterial is robust enough to retain its shape during circulation in vivo and after cell internalization. This is in contrast to softer structures, such as elongated filomicelles, which fragment into smaller particles in the cells and during circulation.[14] Overall, these results indicate that magnetic NWs represent an improved nanomaterial platform for targeting and imaging tumors in vivo. In addition to imaging, NWs may also facilitate more efficient delivery of therapeutics to biological targets because of their large surface area, multiple attachment points, and long blood half-life. These findings are important for the design of in vivo multifunctional nanoprobes applicable to the diagnosis and treatment of a range of human diseases.

Experimental

Nanoworms (NWs) were synthesized using a modification of the published preparation of dextran-coated IO nanoparticles [32]. For the NW synthesis, a higher concentration of iron salts and a higher molecular weight dextran (M_W 20,000 or 40,000, Sigma) were used. NWs or NSs with different numbers of free amines were prepared for peptide conjugation by reacting them with different concentrations of aqueous ammonia at room temperature for 48 h [16–18]. The amine number per NW or NS was measured using the SPDP assay [16]. The amine number per NW was calculated assuming that the molecular weight of a NW is 7 times higher than a NS, based on the mean number of aggregated IO cores for one NW observed in the TEM images and supported by the DLS data. The sizes and shapes of NWs, NSs or Micromod were characterized using TEM, AFM, and DLS. The magnetic properties of NWs, NSs, or Feridex were determined using a SQUID magnetometer. The surface charges of NWs or NSs were measured using a Malvern Instruments Zetasizer equipped with an autotitrator. MRI signals of NWs or NSs were analyzed using a Bruker 4.7 T magnet system.

One targeting peptides were used with the NW or NS samples: KDEPQRRSARLSAKPAPPKPEPKPKKAPAKK (F3), which preferentially binds to blood

vessels and tumor cells in various tumors [36]. The fluorescein (FITC)-conjugated peptides were synthesized using Fmoc chemistry in a solid-phase synthesizer, and purified by preparative HPLC. Their sequence and composition were confirmed by mass spectrometry. An extra cysteine residue was added to the N-terminus to allow conjugation to the aminated dextran coating of the NWs or NSs. For NIR fluorescence imaging, NWs or NSs were first labeled with Cy5.5/Cy7 (one Cy5.5/Cy7 dye per one IO core). The remaining free amines were used for conjugation with the targeting peptides. The number of FITC-peptides or Cy5.5/Cy7 dyes per single NW or NS was determined from the absorbance spectrum. For the cell uptake study, NW-42-F, NW-175-F, and NW-350-F display similar numbers of F3 targeting peptides per iron atom compared with NS-7-F, NS-30-F, and NS-59-F, respectively. Additionally, peptide conjugation to the particles through PEG chains resulted in fewer peptides per particle (Table 1).

For cell internalization tests, MDA-MB-435 cells were seeded into 24-well plates (10,000 per well) and cultured overnight. The cells were then incubated with Cy7-labeled NW-F or NS-F (40 μg (total Fe content) per well) for 30 min, 1 h, or 2 h at 37 °C in the presence of 10% FBS. The wells were rinsed three times with cell media and then imaged in the Cy7 channel (750nm excitation/800 nm emission) with a NIR fluorescence scanner (LI-COR biosciences). The total number of attached Cy7 dye molecules was controlled to yield the same fluorescence intensity on a per-iron basis for both types of particles. The relative fluorescence of the images (each well) was analyzed using the ImageJ (NIH) or OsiriX (Apple) programs.

NW or NS in PBS (100 μL) were intravenously injected into mice (3 mg Fe kg^{-1}). Blood samples were extracted at several different times and magnetization and fluorescence intensities were analyzed by SQUID or by NIR fluorescence, respectively. The blood half-lives of NW and NS were calculated by fitting the fluorescence or magnetization data to a single-exponential equation using a one-compartment open pharmacokinetic model [17]. To determine tissue bio-distribution of the unmodified NW, percentages of injected dose per wet weight of each organ were quantified in healthy tumor-bearing mice.

For *in vivo* passive tumor targeting, mice bearing MDA-MB-435 tumors were anesthetized with intraperitoneal Avertin, and NW or NS (1 mg Fe kg^{-1} body weight in 100 μL PBS) were injected into the tail vein. For real-time observation of tumor/liver uptake, the mice were imaged under anesthesia using NIR fluorescence imaging (Siemens). To quantify NW or NS homing, tumors collected 24 h post injection were analyzed for magnetization using SQUID [45]. All animal work was reviewed and approved by the Burnham Institute's Animal Research Committee (see Supporting Information for details).

Supplementary Material

Refer to Web version on PubMed Central for supplementary material.

References

1. Akerman ME, Chan WCW, Laakkonen P, Bhatia SN, Ruoslahti E. Proc. Natl. Acad. Sci. USA. 2002; 99:12617. [PubMed: 12235356]
2. Gao XH, Cui YY, Levenson RM, Chung LWK, Nie SM. Nat. Biotechnol. 2004; 22:969. [PubMed: 15258594]
3. Ferrari M. Nat. Rev. Cancer. 2005; 5:161. [PubMed: 15738981]
4. Sengupta S, Eavarone D, Capila I, Zhao GL, Watson N, Kiziltepe T, Sasisekharan R. Nature. 2005; 436:568. [PubMed: 16049491]

5. Weissleder R, Kelly K, Sun EY, Shtatland T, Josephson L. Nat. Biotechnol. 2005; 23:1418. [PubMed: 16244656]
6. Seo WS, Lee JH, Sun XM, Suzuki Y, Mann D, Liu Z, Terashima M, Yang PC, McConnell MV, Nishimura DG, Dai HJ. Nat. Mater. 2006; 5:971. [PubMed: 17115025]
7. Lee JH, Jun YW, Yeon SI, Shin JS, Cheon J. Angew. Chem. Int. Ed. 2006; 45:8160.
8. Farokhzad OC, Cheng JJ, Teply BA, Sherifi I, Jon S, Kantoff PW, Richie JP, Langer R. Proc. Natl. Acad. Sci. USA. 2006; 103:6315. [PubMed: 16606824]
9. Cai WB, Shin DW, Chen K, Gheysens O, Cao QZ, Wang SX, Gambhir SS, Chen XY. Nano Lett. 2006; 6:669. [PubMed: 16608262]
10. Lewis JD, Destito G, Zijlstra A, Gonzalez MJ, Quigley JP, Manchester M, Stuhlmann H. Nat. Med. 2006; 12:354. [PubMed: 16501571]
11. Simberg D, Duza T, Park JH, Essler M, Pilch J, Zhang LL, Derfus AM, Yang M, Hoffman RM, Bhatia S, Sailor MJ, Ruoslahti E. Proc. Natl. Acad. Sci. USA. 2007; 104:932. [PubMed: 17215365]
12. Lee JH, Huh YM, Jun Y, Seo J, Jang J, Song HT, Kim S, Cho EJ, Yoon HG, Suh JS, Cheon J. Nat. Med. 2007; 13:95. [PubMed: 17187073]
13. Liu Z, Cai WB, He LN, Nakayama N, Chen K, Sun XM, Chen XY, Dai HJ. Nat. Nanotechnol. 2007; 2:47. [PubMed: 18654207]
14. Geng Y, Dalhaimer P, Cai S, Tsai R, Tewari M, Minko T, Discher DE. Nat. Nanotechnol. 2007; 2:249. [PubMed: 18654271]
15. Shen T, Weissleder R, Papisov M, Bogdanov A, Brady TJ. Magn. Reson. Med. 1993; 29:599. [PubMed: 8505895]
16. Josephson L, Tung CH, Moore A, Weissleder R. Bioconjugate Chem. 1999; 10:186.
17. Wunderbaldinger P, Josephson L, Weissleder R. Bioconjugate Chem. 2002; 13:264.
18. Josephson L, Kircher MF, Mahmood U, Tang Y, Weissleder R. Bioconjugate Chem. 2002; 13:554.
19. Harisinghani MG, Barentsz J, Hahn PF, Deserno WM, Tabatabaei S, van de Kaa CH, de la Rosette J, Weissleder R. N. Engl. J. Med. 2003; 348:2491. [PubMed: 12815134]
20. Weissleder R, Bogdanov A, Neuwelt EA, Papisov M. Adv. Drug Delivery Rev. 1995; 16:321.
21. Jun YW, Huh YM, Choi JS, Lee JH, Song HT, Kim S, Yoon S, Kim KS, Shin JS, Suh JS, Cheon J. J. Am. Chem. Soc. 2005; 127:5732. [PubMed: 15839639]
22. Ai H, Flask C, Weinberg B, Shuai X, Pagel MD, Farrell D, Duerk J, Gao JM. Adv. Mater. 2005; 17:1949.
23. Jun YW, Choi JS, Cheon J. Angew. Chem. Int. Ed. 2006; 45:3414.
24. Xia YN, Halas NJ. MRS Bull. 2005; 30:338.
25. Fu AH, Gu WW, Boussert B, Koski K, Gerion D, Manna L, Le Gros M, Larabell CA, Alivisatos AP. Nano Lett. 2007; 7:179. [PubMed: 17212460]
26. Champion JA, Mitragotri S. Proc. Natl. Acad. Sci. USA. 2006; 103:4930. [PubMed: 16549762]
27. Chithrani BD, Ghazani AA, Chan WCW. Nano Lett. 2006; 6:662. [PubMed: 16608261]
28. Chithrani BD, Chan WCW. Nano Lett. 2007; 7:1542. [PubMed: 17465586]
29. Singh R, Pantarotto D, Lacerda L, Pastorin G, Klumpp C, Prato M, Bianco A, Kostarelos K. Proc. Natl. Acad. Sci. USA. 2006; 103:3357. [PubMed: 16492781]
30. Mammen M, Choi SK, Whitesides GM. Angew. Chem. Int. Ed. 1998; 37:2755.
31. Walsh D, Arcelli L, Ikoma T, Tanaka J, Mann S. Nat. Mater. 2003; 2:386. [PubMed: 12764358]
32. Palmacci, S.; Josephson, L. US Patent. 5262176. 1993.
33. Petit C, Russier V, Pileni MP. J. Phys. Chem. B. 2003; 107:10333.
34. Banerjee IA, Shima LYM, Yoshino T, Takeyama H, Matsunaga T, Matsui H. Adv. Mater. 2005; 17:1128.
35. Perez JM, Josephson L, O'Loughlin T, Hogemann D, Weissleder R. Nat. Biotechnol. 2002; 20:816. [PubMed: 12134166]
36. Porkka K, Laakkonen P, Hoffman JA, Bernasconi M, Ruoslahti E. Proc. Natl. Acad. Sci. USA. 2002; 99:7444. [PubMed: 12032302]

37. Christian S, Pilch J, Akerman ME, Porkka K, Laakkonen P, Ruoslahti E. J. Cell Biol. 2003; 163:871. [PubMed: 14638862]

38. Reddy GR, Bhojani MS, McConville P, Moody J, Moffat BA, Hall DE, Kim G, Koo YEL, Woolliscroft MJ, Sugai JV, Johnson TD, Philbert MA, Kopelman R, Rehemtulla A, Ross BD. Clin. Cancer Res. 2006; 12:6677. [PubMed: 17121886]

39. Moghimi SM, Hunter AC, Murray JC. Pharm. Rev. 2001; 53:283. [PubMed: 11356986]

40. Tang Z, Kotov NA. Adv. Mater. 2005; 17:951.

41. Nikolic MS, Krack M, Aleksandrovic V, Kornowski A, Forster S, Weller H. Angew. Chem. Int. Ed. 2006; 45:6577.

42. DeVries GA, Brunnbauer M, Hu Y, Jackson AM, Long B, Neltner BT, Uzun O, Wunsch BH, Stellacci F. Science. 2007; 315:358. [PubMed: 17234943]

43. Montet X, Funovics M, Montet-Abou K, Weissleder R, Josephson L. J. Med. Chem. 2006; 49:6087. [PubMed: 17004722]

44. Hong S, Leroueil PR, Majoros IJ, Orr BG, Baker JR Jr, Banaszak Holl MM. Chem. Biol. 2007; 14:107. [PubMed: 17254956]

45. GrassiSchultheiss PP, Heller F, Dobson J. Biometals. 1997; 10:351. [PubMed: 9353885]

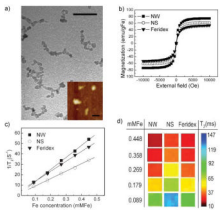

Figure 1.

Physical properties of magnetic NWs and conventional spherical nanoparticles (nanospheres; NSs) preparations. a) TEM image showing the wormlike nanostructure. More than 80% of the particles have a contorted linear appearance with a hydrodynamic length of 50–80 nm. Scale bar is 30 nm. (Inset: atomic force microscopy image showing the elongated shape. Scale bar is 100 nm). b) Magnetization curves for NWs, NSs, and Feridex. c) T_2 relaxation rates as a function of iron concentration (m_M Fe) for NWs, NSs, and Feridex. d) T_2-weighted MR images of NWs, NSs, and Feridex with different concentrations.

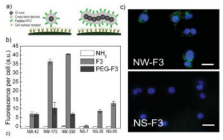

Figure 2.

Internalization of nanoworms (NWs) and nanospheres (NSs) conjugated with F3 peptides into MDA-MB-435 cells. a) Conceptual scheme illustrating the increased multivalent interactions expected between receptors on a cell surface and targeting ligands on a NW compared with a NS. b) Fluorescence data comparing the efficiency of cellular internalization for various functionalized NW and NS systems. NH_2, F3, and PEG-F3 indicate aminated NW/NS, F3-conjugated NW/NS and PEGylgated F3-conjugated NW/NS, respectively. c) Fluorescence microscope images of cells 3 h after incubation with F3(FITC)-conjugated NW (NW-175-F) or F3(FITC)-conjugated NS (NS-30-F) (green). Nuclei are visualized with a DAPI stain (blue). Scale bar is 20 μm.

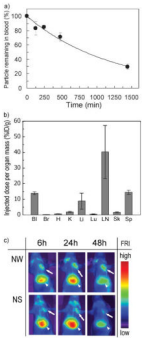

Figure 3.

In vivo behavior of untargeted nanoworms (NWs) in the mouse. a) Percentage of NW remaining in circulation as a function of time with an injection dose (ID) of 3 mgFe kg^{-1}. The solid line represents an exponential fit. b) Biodistribution of NW 24 h post injection. Bl, blood; Br, brain; H, heart; K, kidneys; Li, liver; Lu, lungs; LN, lymph node; Sk, skin; and Sp, spleen. c) Fluorescence images of mice bearing MDA-MB-435 tumors, obtained 6, 24, and 48 h after injection of NW or NS with an ID of 1 mg Fe kg^{-1}. Arrows and arrowheads point to the tumors and the livers, respectively.

Table 1

Characteristics of nanoworms (NWs) and nanospheres (NSs).

Sample [a]	Size [b] [nm]	Blood $T_{1/2}$ [c] [min]	Amine [per NW/NS]	Peptide [per NW/NS]	Peptide [per g Fe ($\times 10^{20}$)]
NS	30.3	1060	0	0	0
NS-7-F	39.2		7	5	2.6
NS-30-F	39.6		30	10	5.3
NS-59-F	41.0		59	12	6.3
NW	65.8	990	0	0	0
NW-42-F	73.7		42	23	1.7
NW-P42-F	87.3		42	16	1.2
NW-175-F	76.6		175	69	5.1
NW-P175-F	88.2		175	48	3.0
NW-350-F	76.1		350	83	6.2
NW-P350-F	90.8		350	59	4.4

[a] The number after the letter identifier designates the number of amine groups per particle. The letter P indicates a poly(ethylene glycol) spacer is used. The –F suffix denotes F3-conjugated particle.

[b] Hydrodynamic size based on DLS measurement (mean size resulting from three measurements).

[c] Relative error in these measurements is ± 10%.